THE JOURNAL OF PHYSICAL CHEMISTRY LETTERS
A JOURNAL OF THE AMERICAN CHEMICAL SOCIETY

pubs.acs.org/JPCL
Letter

Ab Initio Atomistic Characterization of Confined Bulk and Bennett Plasmons in Metallic Nanoparticles as Probed by Penetrating Electrons

Bruno Candelas,△ Mattin Urbieta,△ Antton Babaze, Eduardo Ogando, Andrei G. Borisov, Nerea Zabala, and Javier Aizpurua*

Cite This: *J. Phys. Chem. Lett.* 2025, 16, 2965−2971

Read Online

ACCESS | Metrics & More | Article Recommendations | Supporting Information

ABSTRACT: Despite the experimental observation of confined bulk plasmons (CBPs) in metallic nanostructures using electron energy-loss spectroscopy (EELS), there is still a limited theoretical understanding of their resonance structure when they are excited by penetrating electron beams. In this work, we use atomistic *ab initio* time-dependent density functional theory (TDDFT) to perform a first-principles study of the excitation of CBPs induced by swift electrons. Our quantum approach offers a parameter-free framework for the calculation of the EEL spectra of metallic nanoparticles with atomistic resolution, while jellium TDDFT and classical hydrodynamic calculations allow us to unravel the rich spectral pattern associated with CBPs. Additionally, the excitation of high-energy surface resonances characterized by an induced dipole moment across the nanoparticle surface, known as Bennett modes, is also explored. This study represents a significant step forward in the exploration of plasmonic signatures in the EELS of metallic nanoparticles.

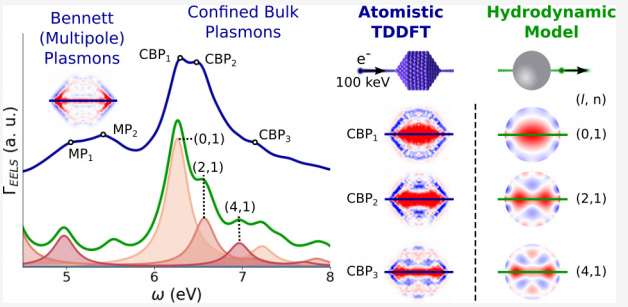

Confined bulk plasmons (CBPs) are longitudinal collective oscillations of the electron density confined within the volume of a nanostructure. Unlike localized surface plasmons (LSPs), CBPs are hardly detected using standard optical spectroscopy techniques due to their inefficient coupling with light,[1−3] and as a result, they have received limited attention in the literature over the years. Nevertheless, recent research has proposed exploiting bulk plasmon excitations in various applications, including the precise measurement of the local temperature at the nanoscale.[4−6] Electron energy-loss spectroscopy (EELS) in state-of-the-art scanning transmission electron microscopes (STEM) has been demonstrated to be a very powerful technique to map the full spectrum of plasmon modes with submillielectronvolt energy and atomic-scale spatial resolution. In addition to the LSPs that have received the most attention, CBPs are effectively excited by swift electron beams that penetrate the sample and longitudinally perturb the electron cloud, as pointed out by recent theoretical work[7] and demonstrated across a variety of structures and materials, including thin Mg films,[8] Ge nanorods,[9] Bi nanowires,[10] Bi nanoparticles,[11,12] and Al nanodisks.[13]

Although the dispersion relation of CBPs in small nanoparticles (NPs) and other nanostructures has been theoretically explored,[1,3,14,15] a complete picture of their excitation by penetrating electron beams in small NPs has not been fully accounted for. Moreover, the limitations of the more widespread local approaches[16] emerge when the size of the NPs approaches a few nanometers, as these frameworks do not describe effects linked to the atomistic structure,[17−19] quantum confinement,[20] nonlocal dynamical screening,[21−23] or variations of the electron density at the surface,[24−26] which significantly influence the plasmonic response. In this context, further theoretical insight that expands the current understanding[3,7] is required to clarify the impact of all of these effects on CBPs.

In this work, we use an *ab initio* atomistic time-dependent density functional theory (TDDFT) framework,[27,28] which has been demonstrated to be a very efficient tool to investigate the sensitivity of valence EELS to the atomistic structure of tiny metallic NPs.[7] We explore in depth the nature of the CBP excitations induced by 100 keV electrons penetrating Na NPs of icosahedral shape and different sizes (given by an average radius r = 1−2.5 nm). Sodium is particularly suited for this study because its electromagnetic response is primarily governed by conduction electrons and therefore it is an excellent free-electron metal prototype, which clearly reveals

Received: January 17, 2025
Revised: March 1, 2025
Accepted: March 5, 2025
Published: March 14, 2025

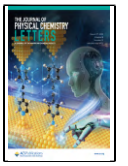

the aforementioned quantum phenomena. Moreover, the free-electron character of sodium enables the comparison of the atomistic TDDFT results with those of alternative jellium TDDFT and hydrodynamic approaches also employed here, allowing us to perform a comprehensive analysis of quantum and nonlocal effects. The atomistic TDDFT EEL probability $\Gamma_{EELS}(\omega)$ for excitation of energy $\hbar\omega$ with Planck's constant $\hbar$ and angular frequency of excitation ω is calculated within the linear-response approximation and semilocal functionals, using the PyNAO code,[27,28] as detailed in ref 7. More specifically, $\Gamma_{EELS}(\omega)$ is computed from the Fourier transform of the external potential due to the electron beam, $\delta V_{ext}(\mathbf{r}, \omega)$, and the charge density it induces in the NP, $\delta n(\mathbf{r}, \omega)$, through the integral $\Gamma_{EELS}(\omega) = \frac{e}{\hbar\pi}\mathrm{Im}\int \delta V^*_{ext}(\mathbf{r}, \omega)\delta n(\mathbf{r}, \omega)\, d\mathbf{r}$. From now on, we will be using atomic units ($\hbar = e = m_e = 1$).

Figure 1a shows the calculated EEL spectra for central electron trajectories through sodium NPs of icosahedral shape[29] and different sizes, ranging from $r \approx 1$ nm (147 atoms) to $r \approx 2.5$ nm (2057 atoms), such that their atomistic structures minimize the ground-state energy. An artificial broadening of 0.1 eV has been considered in these calculations. Notice that for the smallest NP considered (147 atoms; $r \approx 1$ nm), the spectrum is dominated by several peaks due to single electron−hole pair excitations, but as the particle size increases, three well-defined collective peaks emerge. The lowest-energy peaks (∼3.1 eV) correspond to LSPs, which were previously studied in the optical response[30] and EELS,[7] with the main contribution being the quadrupolar LSP, as evidenced by the induced charge density color plot shown in the inset. Notice that, as the NP size decreases, the resonant energies of LSPs remain quite stable, with a slight blue-shift. At higher energies (∼5.2 eV), another set of peaks emerges (see the corresponding induced charge density in the inset). These are identified as Bennett plasmons,[31] also known as multipole plasmons[32,33] (MPs). The emergence of these modes deserves further attention, and we analyze them in greater detail below.

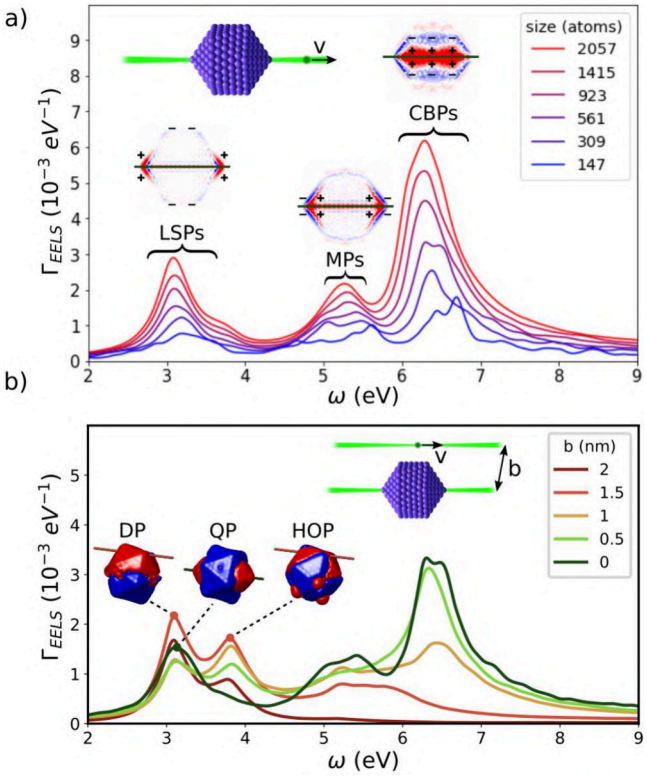

Figure 1. EEL spectra calculated with atomistic *ab initio* TDDFT for 100 keV electrons probing icosahedral sodium NPs. (a) The different colors correspond to spectra for central electron trajectories ($b = 0$ nm) through NPs of different size or numbers of atoms, ranging from 147 atoms ($r \approx 1$ nm) to 2057 atoms ($r \approx 2.5$ nm). The three main peaks labeled in the spectra correspond to localized surface plasmons (LSPs), Bennett or multipole plasmons (MPs), and confined bulk plasmons (CPBs). The insets display schematics of the electron beam incidence and 2D plots of the cross-sectional views of the induced charge density distribution of the LSP, MP, and CBP resonances for the Na_{2057} NP. The red and blue colors in the induced charge densities refer to positive and negative values, respectively. (b) EELS spectra for a Na_{561} ($r \approx 1.6$ nm) NP for electron trajectories with different impact parameters b. The insets depict schematics of the impact parameter and 3D isosurfaces of induced charge densities for the three different LSPs emerging in the spectra.

The most prominent peaks (∼6.3 eV) in the EEL spectra shown in Figure 1a are close to the plasma frequency ω_p of Na and correspond to charge density oscillations confined within the volume of the NP, so-called CBPs,[7] as demonstrated by the two-dimensional (2D) plots of the induced charge density cross-sectional view displayed in the inset. They are characterized by a series of satellite peaks and shoulders, evidencing the complex nature of the CBP excitations (details below). Moreover, the EEL spectra for the Na_{561} NP ($r \approx 1.6$ nm) shown in Figure 1b demonstrate that, while surface plasmons are excited by both penetrating and aloof electron beam trajectories, CBPs are efficiently excited only by beam trajectories that penetrate the NP, with the impact parameter b determining which modes are activated and how intensely. Additionally, the impact parameter strongly affects the excitation of LSP modes, as was reported in ref 7. For central trajectories, the quadrupolar LSP dominates the spectrum but there is a gradual transition to the excitation of the dipolar LSP as the impact parameter increases. For grazing trajectories, higher-order modes are also excited, which were not visible for the central trajectory. We depict the three-dimensional (3D) isosurfaces of the induced charge densities corresponding to these three LSP modes in the insets of Figure 1b.

Although *ab initio* atomistic TDDFT offers a state-of-the-art parameter-free platform for calculating the EEL spectra in small NPs,[7] the interpretation of the results is challenging due to the overlapping of different resonances, particularly at CBP energies. In order to shed light and guide the characterization of the modal composition of CBP resonances, we also compute $\Gamma_{EELS}(\omega)$ for a reference spherical Na NP of the same size using two additional models accounting for nonlocal effects. First, we obtain the optical response of the NP within an analytical hydrodynamic model (HDM),[34,35] which describes the NP as a compressible electron gas ($r_s = 2.08$ Å; $\omega_p \approx 6.05$ eV) confined within a sphere of hard boundaries (zero current perpendicular to the interface and no surface charge density outside the boundaries) preventing the electron spill-out, as previously employed for EELS calculations considering aloof electron trajectories.[3] In Figure 2a, we plot $\Gamma_{EELS}(\omega)$ for a reference NP of radius $r = 2.13$ nm in the CBP spectral range, highlighting the contribution of each angular momentum l component.

To address the adequacy of the HDM in describing the excitation of CBPs, we perform additional calculations of the EEL probability using the jellium model of free-electron metals

https://doi.org/10.1021/acs.jpclett.5c00157
J. Phys. Chem. Lett. 2025, 16, 2965−2971

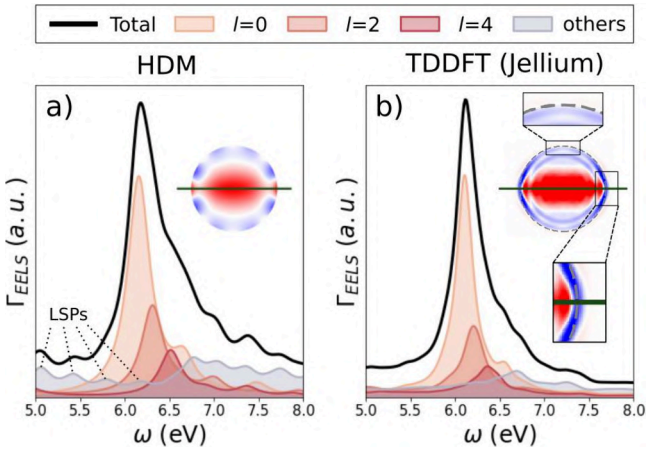

Figure 2. EEL spectra for 100 keV electrons passing through the center of a spherical Na NP calculated with two different approaches. (a) HDM results for a reference Na spherical NP of radius r = 2.13 nm. The contributions of the main l components are distinguished with different colors. The 2D cross-sectional view of the induced charge density at the main CBP resonance energy is displayed in the inset (red for positive charge and blue for negative charge). (b) TDDFT results within the jellium model for a reference spherical Na NP containing 1074 conduction electrons. The inset shows the 2D induced charge density cross-sectional view computed at the main CBP resonance energy. The dashed line represents the boundary of the background positive charge density of the jellium sphere. The magnified insets at the bottom and top outline the spill-out of the electron cloud at the surface around the electron path and far from it, respectively.

and the TDDFT formalism[36,37] as implemented in our previous work,[38,39] which is depicted in Figure 2b. Within the jellium model, the metallic ions are represented as a positively charged background with homogeneous density while conduction electrons are treated as interacting particles confined within the self-consistent spherical potential well in the TDDFT formalism. This formalism allows for describing variations of the induced charge density near the NP's surface associated with a finite potential barrier and thus the electron spill-out at the metal−vacuum interface, an effect that the hard-boundary HDM cannot capture.[40] The simplified quantum description of the jellium electron gas excludes features captured by the atomistic TDDFT calculations related to the precise atomistic structure and to the nonspherical shape of the NP, while still accurately accounting for the nonlocal effects in the dynamics of conduction electrons that the HDM seeks to address. As one can appreciate in Figure 2a, the hard-boundary nature of the HDM leads to a systematic blue-shift of LSPs, with the presence of artificial resonance features close to the bulk plasma frequency ω_p, together with differences in the induced charge density at the surface (compare the insets of panels a and b of Figure 2). However, despite these limitations, the HDM properly accounts for the nonlocal plasmonic response in the volume of the NP, since both the HDM and the jellium TDDFT model consistently predict that CBP resonances are formed by several volume modes with different angular momenta l. This agreement proves the utility of the HDM in identifying the CBPs excited in small NPs using analytical expressions and minimal computational resources.

With the help of the HDM model, we can now characterize the complex CBP modal structure observed in the atomistic TDDFT results. We focus on the Na_{561} ($r \approx 1.6$ nm) NP, as it is the largest one for which the excitation of distinct CBP modes can be clearly observed in the EEL probability spectra. Figure 3 compares the atomistic TDDFT (panel a) and HDM (panel b) Γ_{EELS} calculations, for increasing impact parameters b of the electron beam trajectory. For the central trajectory (b = 0), multiple CBP peaks are identified and labeled as CBP_j with $j = \{1, 2, 3\}$ in Figure 3a. By comparing these spectra with the corresponding HDM results in Figure 3b, it is possible to identify a correspondence between the CBP peaks of the atomistic TDDFT and the well-defined spectral modes of the HDM. These modes are labeled as (l, n), where l is related to the angular distribution of the induced charge density and n is the number of nodes in the radial direction. The main peak CBP_1 at 6.3 eV corresponds to the $(l, n) = (0, 1)$ mode, the subsequent peak CBP_2 at 6.5 eV to the $(2, 1)$ mode, and CBP_3 at 7.1 eV to the $(4, 1)$ mode. The excellent matching between the atomistic TDDFT and HDM results is further demonstrated through the visualization of the isosurfaces of the induced charge densities and their cross-sectional views along different planes in panels a and b of Figure 4, reinforcing the consistent relationship between CBP peaks and specific (l, n) modes. Notice that for the axial trajectory, b = 0, only even values of l contribute to the EEL probability.[35]

Next, we extend our analysis to noncentral beam trajectories ($b \neq 0$), which cause significant changes in the spectral shape of Γ_{EELS}, as shown in Figure 3. First, the overall contribution of

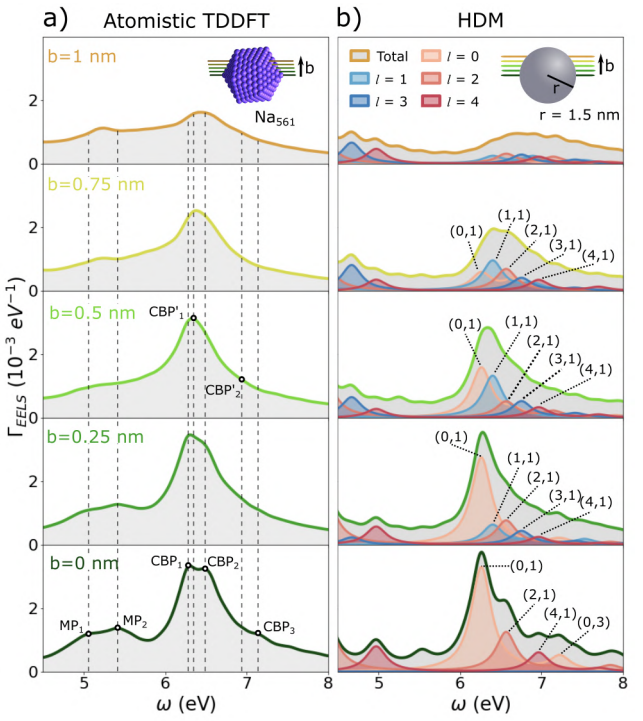

Figure 3. High-energy part of the EELS spectra for 100 keV electron trajectories, highlighting the excitation of bulk plasmon modes. Results calculated with (a) the atomistic TDDFT formalism and (b) the HDM through (a) an icosahedral Na_{561} NP and (b) a spherical Na NP (r = 1.5 nm) are shown for different electron trajectories characterized by their impact parameters b, as sketched in the inset. The different modes are labeled as CBP_j (confined bulk plasmons) and MP_j (Bennett or multipole plasmons), with j being the order of the mode. The contributions of the (l, n) modes in the HDM spectra are displayed separately, using different colors to distinguish even and odd contributions.

https://doi.org/10.1021/acs.jpclett.5c00157
J. Phys. Chem. Lett. 2025, 16, 2965−2971

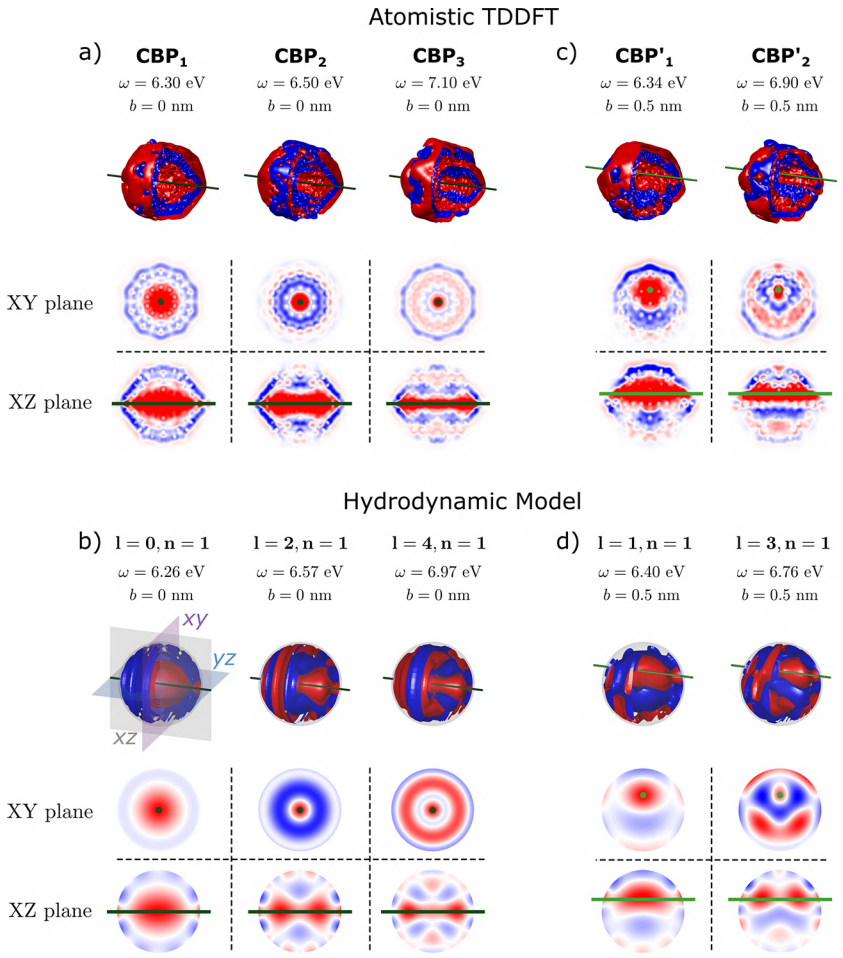

Figure 4. 3D isosurfaces of the induced charge densities for the CBP resonances excited by a central electron beam trajectory (b = 0 nm) through (a) a Na_{561} NP, calculated with atomistic TDDFT, and (b) a reference spherical sodium NP (r = 1.5 nm), calculated with the HDM. The 3D images show isosurfaces of the induced charge density for each of the modes (with a quarter of the NP removed), whereas the 2D plots show cross-sectional views of the induced density along the $X-Y$ and $X-Z$ planes. Each of the HDM modes is labeled with its corresponding l and n numbers. Note that, while the main contributions at these energies correspond to the labeled modes, there are also contributions from other overlapping modes, and thus, the induced densities do not strictly follow the symmetry associated with the (l, n) mode. (c) Same as panel a but for impact parameter b = 0.5 nm. (d) Same as panel b but for impact parameter b = 0.5 nm.

the CBP modes to the Γ_{EELS} spectrum decreases with an increase in b, because the incident electron's path inside the NP is shorter. Second, the resonance profile of the EEL probability spectrum changes, in concordance with the loss of the rotational symmetry of the induced charge density (C_5 rotation around a vertex−vertex axis for the atomistic icosahedral nanoparticles and azimuthal symmetry for the spherical ones) that can be seen in panels c and d of Figure 4. The main spectral changes observed are the blue-shift of the peak associated with the overlapping CBP modes and the smoothening of the higher-energy peaks, which become less prominent. We label the new peaks emerging for noncentral electron trajectories, corresponding to a sum of contributions of several multipolar resonances, as CBP'_1 and CBP'_2. The observed trends are understood by examining the corresponding HDM spectra, which reveal that the overall shift of the spectrum is driven by the excitation of odd-l modes, forbidden for central trajectories due to symmetry constraints.[35] As a result of the rotational symmetry breaking when the electron trajectory departs from the center of the NP, the main peak blue-shifts as the (0, 1) mode is gradually surpassed in intensity by the (1, 1) mode emerging at a slightly higher energy. Simultaneously, the excitation of odd-l CBP modes overlapping with the even-l ones smoothens the high-energy tail of the EEL probability spectra, which explains the difficulty to identify the separate modes in the atomistic TDDFT results. The spatial characterization of odd-l CBP modes, activated by the symmetry breaking of noncentral trajectories, is more clearly illustrated in panels c and d of Figure 4, where the isosurfaces of the induced charge densities for the main spectral peaks are displayed for nonaxial electron trajectories. The excellent matching of the atomistic TDDFT and HDM patterns is evident upon comparison of panels a (modes CBP_1, CBP_2, and CBP_3) and b (HDM modes (0, 1), (2, 1), and (4, 1)) for the b = 0 trajectory and panels c (modes CBP'_1 and CBP'_2) and d (HDM modes (1, 1) and (3, 1)) for the nonaxial b = 0.5 nm trajectory.

To conclude, we examine the spectral features emerging between the LSP and CBP modes in the atomistic TDDFT Γ_{EELS} spectra, labeled as MP_1 and MP_2 in Figure 3a and corresponding to Bennett plasmons.[31] While LSPs are characterized by a resonant charge oscillation distributed over the whole NP surface, the Bennett plasmons correspond to a resonant dipole moment formed by induced charge

https://doi.org/10.1021/acs.jpclett.5c00157
J. Phys. Chem. Lett. 2025, 16, 2965−2971

densities of opposite sign across the NP boundary[2,41] (see panels b and c of Figure 5). With the aim of exploring the nature of these modes and their differences with the LSP and CBP modes described previously, we introduce the accumulated charge ratio, $R_q(\rho, \omega)$, which measures the ratio of the total (atomistic TDDFT) induced charge in absolute value contained within a spherical shell of radius ρ:

$$R_q(\rho, \omega) = \frac{\int_0^{\rho} \rho'^2 |\delta n(\rho', \phi, \theta, \omega)| \sin\theta \, d\rho' \, d\phi \, d\theta}{\int_0^{\infty} \rho'^2 |\delta n(\rho', \phi, \theta, \omega)| \sin\theta \, d\rho' \, d\phi \, d\theta} \quad (1)$$

where $\delta n(\rho', \phi, \theta, \omega)$ is the induced charge density in spherical coordinates (ρ', ϕ, θ) at excitation energy ω.

Figure 5a shows the calculated $R_q(\rho, \omega)$ as a function of ρ for all of the volume and surface modes studied throughout this work for the Na_{561} NP and a central electron trajectory. The dashed black line corresponds to a homogeneous spherical charge distribution, i.e., $R_q(\rho, \omega) = \rho^3/r^3$, plotted for reference.

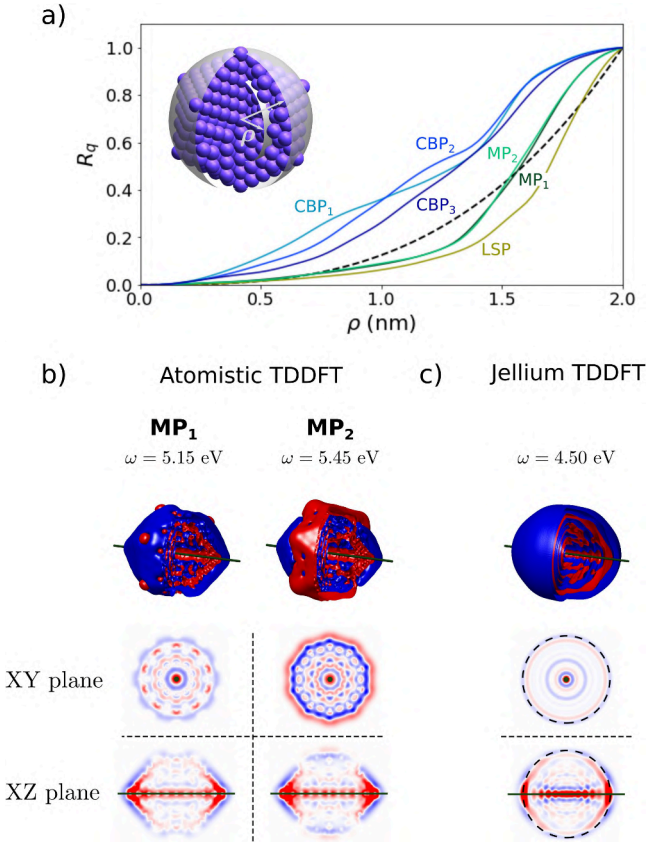

Figure 5. (a) Accumulated charge ratio $R_q(\rho, \omega)$ computed according to eq 1 for various modes excited by an electron beam with $b = 0$ for the Na_{561} NP as a function of spherical shell radius ρ. The results corresponding to LSP modes are shown by yellow lines, those corresponding to Bennett or MP modes by green lines, and those corresponding to CBP modes by blue lines, with the homogeneous charge density reference depicted as a dashed black line. The inset depicts the spherical shells used for the computation of $R_q(\rho, \omega)$. (b) Atomistic TDDFT results of the induced charge density for the two MP (or Bennett) modes, displaying both 3D isosurfaces (with one-quarter removed) and cross-sectional views along the $X-Y$ and $X-Z$ planes. (c) Same as panel b but for TDDFT results obtained within the jellium model. The dashed lines represent the boundaries of the background positive charge density in the jellium calculations.

From the comparison, it is clear that the induced charge of the CBP modes (blue lines) is accumulated inside the volume of the NP while the LSP mode (yellow line) exhibits an induced density distribution skewed toward the surface. Importantly, Bennett plasmons MP_1 and MP_2 (green lines) exhibit a behavior similar to the LSP, with a slightly deeper penetration into the NP, thus confirming their surface nature. Figure 5b shows the isosurfaces of the induced charge densities obtained from atomistic TDDFT calculations for the MP_1 and MP_2 modes, which exhibit the characteristic distribution of Bennett plasmons.[41] The excitation of Bennet plasmons by penetrating electron trajectories is also supported by TDDFT calculations based on the jellium model employed in Figure 2b, which predict the emergence of several resonances between the LSPs and the CBPs, at frequencies consistent with our previous studies.[23] As an example, Figure 5c depicts the induced charge density at the lowest-energy resonance (4.5 eV), which shows remarkably good qualitative agreement with the atomistic TDDFT results. Thus, the excitation of Bennett plasmons in small nanoparticles by penetrating electron trajectories is robustly demonstrated, although quantitative details might depend on the specific description of the metal surface.

In summary, we employed an atomistic TDDFT framework to investigate the excitation of CBPs in sodium nanoparticles by analyzing the EEL probability. With the help of an analytical HDM model, we have been able to characterize the modal structure of the CBPs excited by electron trajectories penetrating the nanoparticles and to identify the contribution of individual modes to the EEL spectra. Finally, our atomistic and jellium TDDFT studies have also shown that electron beams penetrating the sample can efficiently excite Bennett plasmons at the surface between the LSP and CBP resonance energies, which is missed by the HDM model. The overall good qualitative, and even quantitative, agreement between theoretical models that include nonlocality in the response of the nanoparticles at different levels underscores the robustness of the studied phenomena in small sodium nanoparticles. Furthermore, our study serves to interpret the experimentally observed blue-shift of the bulk peak in Bi nanoparticles[12] and Al disks[13] with increasing impact parameters and to provide a deeper understanding of the behavior of CBPs in metallic nanostructures. The conceptual characterization of CBPs and Bennett plasmons as performed here will allow for a more exhaustive analysis and technological exploitation of plasmonic features in the valence EELS of metal nanoparticles.

■ ASSOCIATED CONTENT

Data Availability Statement

The data that support the findings of this study are available from the corresponding author upon reasonable request. The data set corresponding to the results shown in the figures of this paper can be found at https://digital.csic.es/. The SIESTA[27] code is available at https://gitlab.com/siesta-project/siesta.git. The PyNAO[28] code is available at https://gitlab.com/mbarbry/pynao.git.

Supporting Information

The Supporting Information is available free of charge at https://pubs.acs.org/doi/10.1021/acs.jpclett.5c00157.

Transparent Peer Review report available (PDF)

https://doi.org/10.1021/acs.jpclett.5c00157
J. Phys. Chem. Lett. 2025, 16, 2965−2971

AUTHOR INFORMATION

Corresponding Author

Javier Aizpurua − *Donostia International Physics Center, 20018 Donostia, Spain; Department of Electricity and Electronics, FCT-ZTF, UPV/EHU, 48940 Leioa, Spain; IKERBASQUE, Basque Foundation for Science, 48009 Bilbao, Spain;* orcid.org/0000-0002-1444-7589; Email: aizpurua@ehu.eus

Authors

Bruno Candelas − *Materials Physics Center, CSIC-UPV/EHU, 20018 Donostia, Spain; Donostia International Physics Center, 20018 Donostia, Spain; Department of Electricity and Electronics, FCT-ZTF, UPV/EHU, 48940 Leioa, Spain;* orcid.org/0000-0001-8777-4022

Mattin Urbieta − *Fisika Aplikatua Saila, Vitoria-Gasteizko Ingeniaritza Eskola, UPV/EHU, 01006 Vitoria-Gasteiz, Spain*

Antton Babaze − *Materials Physics Center, CSIC-UPV/EHU, 20018 Donostia, Spain; Donostia International Physics Center, 20018 Donostia, Spain; Department of Applied Physics, School of Architecture, UPV/EHU, 20018 Donostia, Spain;* orcid.org/0000-0002-9775-062X

Eduardo Ogando − *Fisika Saila, Farmazia Fakultatea, UPV/EHU, 01006 Vitoria-Gasteiz, Spain;* orcid.org/0000-0001-5632-1514

Andrei G. Borisov − *Institut des Sciences Moléculaires d'Orsay, UMR 8214, CNRS-Université Paris-Saclay,, 91405 Orsay, France; Donostia International Physics Center, 20018 Donostia, Spain;* orcid.org/0000-0003-0819-5028

Nerea Zabala − *Department of Electricity and Electronics, FCT-ZTF, UPV/EHU, 48940 Leioa, Spain; Materials Physics Center, CSIC-UPV/EHU, 20018 Donostia, Spain; Donostia International Physics Center, 20018 Donostia, Spain;* orcid.org/0000-0002-1619-7544

Complete contact information is available at: https://pubs.acs.org/10.1021/acs.jpclett.5c00157

Author Contributions

△B.C. and M.U. contributed equally to this work.

Notes

The authors declare no competing financial interest.

ACKNOWLEDGMENTS

B.C. acknowledges support through the Ph.D. Student program of the Materials Physics Center and Donostia International Physics Center. The authors also acknowledge support from the Department of Education, Research and Universities of the Basque Government through Project IT1526-22 and Grant PID2022-139579NB-I00 funded by MCIU/AEI/10.13039/501100011033 and ERDF/EU.

REFERENCES

(1) Ruppin, R. Optical properties of a plasma sphere. *Phys. Rev. Lett.* **1973**, *31*, 1434−1437.

(2) Stella, L.; Zhang, P.; García-Vidal, F. J.; Rubio, A.; García-González, P. Performance of Nonlocal Optics When Applied to Plasmonic Nanostructures. *J. Phys. Chem. C* **2013**, *117*, 8941−8949.

(3) Christensen, T.; Yan, W.; Raza, S.; Jauho, A.-P.; Mortensen, N. A.; Wubs, M. Nonlocal Response of Metallic Nanospheres Probed by Light, Electrons, and Atoms. *ACS Nano* **2014**, *8*, 1745−1758.

(4) Mecklenburg, M.; Hubbard, W. A.; White, E. R.; Dhall, R.; Cronin, S. B.; Aloni, S.; Regan, B. C. Nanoscale temperature mapping in operating microelectronic devices. *Science* **2015**, *347*, 629−632.

(5) Mecklenburg, M.; Zutter, B.; Regan, B. C. Thermometry of Silicon Nanoparticles. *Phys. Rev. Appl.* **2018**, *9*, 014005.

(6) Wang, C.; Yang, W.-C. D.; Raciti, D.; Bruma, A.; Marx, R.; Agrawal, A.; Sharma, R. Endothermic reaction at room temperature enabled by deep-ultraviolet plasmons. *Nat. Mater.* **2021**, *20*, 346−352.

(7) Urbieta, M.; Barbry, M.; Koval, P.; Rivacoba, A.; Sánchez-Portal, D.; Aizpurua, J.; Zabala, N. Footprints of atomic-scale features in plasmonic nanoparticles as revealed by electron energy loss spectroscopy. *Phys. Chem. Chem. Phys.* **2024**, *26*, 14991−15004.

(8) Özer, M. M.; Moon, E. J.; Eguiluz, A. G.; Weitering, H. H. A Comprehensive Study of Electron Energy Losses in Ge Nanowires. *Phys. Rev. Lett.* **2011**, *106*, 197601.

(9) Hanrath, T.; Korgel, B. A. Plasmon Response of a Quantum-Confined Electron Gas Probed by Core-Level Photoemission. *Nano Lett.* **2004**, *4*, 1455−1461.

(10) Sander, M. S.; Gronsky, R.; Lin, Y. M.; Dresselhaus, M. S. Plasmon excitation modes in nanowire arrays. *J. Appl. Phys.* **2001**, *89*, 2733−2736.

(11) Wang, Y. W.; Kim, J. S.; Kim, G. H.; Kim, K. S. Quantum size effects in the volume plasmon excitation of bismuth nanoparticles investigated by electron energy loss spectroscopy. *Appl. Phys. Lett.* **2006**, *88*, 143106.

(12) Borja-Urby, R.; Paredes-Carrera, S. P.; Viltres-Cobas, H.; Santiago-Jacinto, P.; Paraguay-Delgado, F.; Herrera-Pérez, G.; Rendón-Vázquez, L.; Sánchez-Ochoa, J. C.; Morales-Cruz, D. Confined volume plasmon spatial distribution by low-loss EELS on self-assemble bismuth nanoparticles. *J. Electron Spectrosc. Relat. Phenom.* **2019**, *237*, 146891.

(13) Hobbs, R. G.; Manfrinato, V. R.; Yang, Y.; Goodman, S. A.; Zhang, L.; Stach, E. A.; Berggren, K. K. High-Energy Surface and Volume Plasmons in Nanopatterned Sub-10 nm Aluminum Nanostructures. *Nano Lett.* **2016**, *16*, 4149−4157.

(14) v. Baltz, R.; Mensch, M. P.; Zohm, H. Longitudinal electric response and loss-function of metallic microspheres and voids. *ZPhys-e.B: Condens. Matter* **1995**, *98*, 151−161.

(15) Raza, S.; Kadkhodazadeh, S.; Christensen, T.; Di Vece, M.; Wubs, M.; Mortensen, N. A.; Stenger, N. Multipole plasmons and their disappearance in few-nanometre silver nanoparticles. *Nat. Commun.* **2015**, *6*, 8788.

(16) Stamatopoulou, P. E.; Zhao, W.; Rodríguez Echarri, A.; Mortensen, N. A.; Busch, K.; Tserkezis, C.; Wolff, C. Electron beams traversing spherical nanoparticles: Analytic and numerical treatment. *Phys. Rev. Res.* **2024**, *6*, 013239.

(17) Varas, A.; García-González, P.; García-Vidal, F. J.; Rubio, A. Anisotropy Effects on the Plasmonic Response of Nanoparticle Dimers. *J. Phys. Chem. Lett.* **2015**, *6*, 1891−1898.

(18) Lafiosca, P.; Giovannini, T.; Benzi, M.; Cappelli, C. Going Beyond the Limits of Classical Atomistic Modeling of Plasmonic Nanostructures. *J. Phys. Chem. C* **2021**, *125*, 23848−23863.

(19) Candelas, B.; Zabala, N.; Koval, P.; Babaze, A.; Sánchez-Portal, D.; Aizpurua, J. Influence of atomistic features in plasmon−exciton coupling and charge transfer driven by a single molecule in a metallic nanocavity. *J. Chem. Phys.* **2024**, *161*, 044707.

(20) Monreal, R. C.; Apell, S. P.; Antosiewicz, T. J. Quantum-size effects in visible defect photoluminescence of colloidal ZnO quantum dots: a theoretical analysis. *Nanoscale* **2018**, *10*, 7016−7025.

(21) García de Abajo, F. J. Nonlocal effects in the plasmons of strongly interacting nanoparticles, dimers, and waveguides. *J. Phys. Chem. C* **2008**, *112*, 17983−17987.

(22) Teperik, T. V.; Nordlander, P.; Aizpurua, J.; Borisov, A. G. Quantum effects and nonlocality in strongly coupled plasmonic nanowire dimers. *Opt. Express* **2013**, *21*, 27306−27325.

(23) Babaze, A.; Neuman, T.; Esteban, R.; Aizpurua, J.; Borisov, A. G. Dispersive surface-response formalism to address nonlocality in extreme plasmonic field confinement. *Nanophotonics* **2023**, *12*, 3277−3289.

(24) Liebsch, A. *Electronic Excitations at Metal Surfaces*; Springer Science & Business Media, 2013.
(25) Ciracì, C.; Della Sala, F. Quantum hydrodynamic theory for plasmonics: Impact of the electron density tail. *Phys. Rev. B* **2016**, *93*, 205405.
(26) Babaze, A.; Ogando, E.; Stamatopoulou, P. E.; Tserkezis, C.; Mortensen, N. A.; Aizpurua, J.; Borisov, A. G.; Esteban, R. Quantum surface effects in the electromagnetic coupling between a quantum emitter and a plasmonic nanoantenna: time-dependent density functional theory vs. semiclassical Feibelman approach. *Opt. Express* **2022**, *30*, 21159−21183.
(27) Soler, J. M.; Artacho, E.; Gale, J. D.; García, A.; Junquera, J.; Ordejón, P.; Sánchez-Portal, D. The SIESTA method for ab initio order-N materials simulation. *J. Phys.: Condens. Matter* **2002**, *14*, 2745.
(28) Koval, P.; Barbry, M.; Sánchez-Portal, D. PySCF-NAO: An efficient and flexible implementation of linear response time-dependent density functional theory with numerical atomic orbitals. *Comput. Phys. Commun.* **2019**, *236*, 188−204.
(29) Noya, E. G.; Doye, J. P.K.; Wales, D. J.; Aguado, A. Geometric magic numbers of sodium clusters: Interpretation of the melting behaviour. *Eur. Phys. J. D* **2007**, *43*, 57−60.
(30) Urbieta, M.; Barbry, M.; Zhang, Y.; Koval, P.; Sánchez-Portal, D.; Zabala, N.; Aizpurua, J. Atomic-Scale Lightning Rod Effect in Plasmonic Picocavities: A Classical View to a Quantum Effect. *ACS Nano* **2018**, *12*, 585−595.
(31) Bennett, A. J. Influence of the Electron Charge Distribution on Surface-Plasmon Dispersion. *Phys. Rev. B* **1970**, *1*, 203.
(32) Tsuei, K.-D.; Plummer, E. W.; Liebsch, A.; Kempa, K.; Bakshi, P. Multipole plasmon modes at a metal surface. *Phys. Rev. Lett.* **1990**, *64*, 44−47.
(33) Yan, W. Hydrodynamic theory for quantum plasmonics: Linear-response dynamics of the inhomogeneous electron gas. *Phys. Rev. B* **2015**, *91*, 115416.
(34) Rivacoba, A. Electron spill-out effects in plasmon excitations by fast electrons. *Ultramicroscopy* **2019**, *207*, 112835.
(35) Urbieta, M. Theoretical approach to atomic-scale nanoplasmonics as probed by light and swift electrons. Ph.D. Thesis, University of the Basque Country, UPV/EHU, Leioa, Spain, 2021.
(36) Brack, M. The physics of simple metal clusters: self-consistent jellium model and semiclassical approaches. *Rev. Mod. Phys.* **1993**, *65*, 677.
(37) Varas, A.; García-González, P.; Feist, J.; García-Vidal, F.; Rubio, A. Quantum plasmonics: from jellium models to ab initio calculations. *Nanophotonics* **2016**, *5*, 409−426.
(38) Borisov, A.; Sánchez-Portal, D.; Díez Muiño, R.; Echenique, P. Building up the screening below the femtosecond scale. *Chem. Phys. Lett.* **2004**, *387*, 95−100.
(39) Zapata Herrera, M.; Aizpurua, J.; Kazansky, A. K.; Borisov, A. G. Plasmon Response and Electron Dynamics in Charged Metallic Nanoparticles. *Langmuir* **2016**, *32*, 2829−2840.
(40) Teperik, T. V.; Nordlander, P.; Aizpurua, J.; Borisov, A. G. Robust Subnanometric Plasmon Ruler by Rescaling of the Nonlocal Optical Response. *Phys. Rev. Lett.* **2013**, *110*, 263901.
(41) Toscano, G.; Straubel, J.; Kwiatkowski, A.; Rockstuhl, C.; Evers, F.; Xu, H.; Asger Mortensen, N.; Wubs, M. Resonance shifts and spill-out effects in self-consisten hydrodinamic nanoplasmonics. *Nat. Commun.* **2015**, *6*, 7132.

https://doi.org/10.1021/acs.jpclett.5c00157
J. Phys. Chem. Lett. 2025, 16, 2965−2971